

Forward Laplacian: A New Computational Framework for Neural Network-based Variational Monte Carlo

Ruichen Li^{1,2§†}, Haotian Ye^{1†}, Du Jiang^{1,2§}, Xuelan Wen², Chuwei Wang¹, Zhe Li², Xiang Li², Di He^{1,a}, Ji Chen^{1,b}, Weiluo Ren^{2,c}, Liwei Wang^{1,d}

¹Peking University.

²ByteDance Research.

Abstract

Neural network-based variational Monte Carlo (NN-VMC) has emerged as a promising cutting-edge technique of *ab initio* quantum chemistry. However, the high computational cost of existing approaches hinders their applications in realistic chemistry problems. Here, we report the development of a new NN-VMC method that achieves a remarkable speed-up by more than one order of magnitude, thereby greatly extending the applicability of NN-VMC to larger systems. Our key design is a novel computational framework named Forward Laplacian, which computes the Laplacian associated with neural networks, the bottleneck of NN-VMC, through an efficient forward propagation process. We then demonstrate that Forward Laplacian is not only versatile but also facilitates more developments of acceleration methods across various aspects, including optimization for sparse derivative matrix and efficient neural network design. Empirically, our approach enables NN-VMC to investigate a broader range of atoms, molecules and chemical reactions for the first time, providing valuable references to other *ab initio* methods. The results demonstrate a great potential in applying deep learning methods to solve general quantum mechanical problems.

1 Main

Accurately solving the time-independent electronic Schrödinger equation can yield the fundamental properties of a given quantum mechanical system. Quantum Monte Carlo (QMC) [1, 2] is one of the most important *ab initio* methods for solving the Schrödinger equation, widely employed in various scenarios in quantum chemistry. However, in QMC, the accuracy of the solution heavily relies on the choice of the ansatz, which requires significant expertise. This limitation restricts the adaptability of QMC compared

to other deterministic approaches, such as CCSD(T), which is widely considered as the “gold standard”.

Recently, deep learning has revolutionized the field of quantum chemistry for obtaining more accurate solutions to the Schrödinger equation. One of the pioneering approaches is Neural Network-based Variational Monte Carlo (NN-VMC), such as FermiNet [3, 4] and PauliNet [5]. The ground state wavefunction can be obtained through the variational principle, by which the expectation value of the energy is minimized. Based on this fact, NN-VMC methods utilize deep neural networks to parameterize the wavefunction and optimize the network parameters with the energy serving as the loss function. Benefiting from the remarkable capacity of neural networks, NN-VMC methods demonstrated promising results to attain chemical accuracy for diverse systems. However, it is essential to note that these methods often incur significant computational costs during model training. For instance, learning a wavefunction for the benzene

[§]These authors carried out this work as interns at ByteDance.

[†]Equal Contribution

^adihe@pku.edu.cn

^bji.chen@pku.edu.cn

^crenweiluo@bytedance.com

^dwanglw@pku.edu.cn

dimer system requires approximately 10,000 GPU hours [6] on modern hardware, making it challenging to scale up toward larger systems.

In this work, we tackle the challenge of computational efficiency in NN-VMC methods, especially for large-scale systems. Note that NN-VMC needs to compute the Laplacian with respect to the neural network input to obtain the loss. Through our investigation, the calculation of this term consumes a substantial proportion of the overall training time and becomes the primary bottleneck in the learning procedure. In detail, previous works first compute the Hessian matrix using the auto differentiation (**AutoDiff**) method in deep learning toolkits and then derive the Laplacian by taking the trace. Such a process requires performing forward propagation and backward propagation multiple times, significantly slowing down the overall training speed of NN-VMC. See Section 4.2 for a detailed analysis.

Observing this problem, we first develop a novel computational framework named Forward Laplacian. In contrast to the commonly used method that indirectly derives the Laplacian from the Hessian, Forward Laplacian directly computes the value through a carefully crafted forward propagation process, which we mathematically show is much more efficient as it eliminates unnecessary computation and propagation. Second, we demonstrate that this way of computation not only accelerates the process but also paves the way for developing advanced techniques in NN-VMC. In particular, we illustrate that in the Forward Laplacian associated with NN-VMC ansatz, many intermediate derivatives exhibit sparsity and can be optimized to a considerable extent. We also design an efficient neural network architecture called LapNet, which can better exploit the strength of the Forward Laplacian method using carefully designed attention blocks with sparse derivatives. Together, these developments allow us to study atoms, molecules, and chemical reactions beyond the capability of existing NN-VMC packages.

In the following sections, we first evaluate our method on a wide range of systems in terms of calculating the absolute energy following [3, 4, 6]. All results consistently indicate that LapNet, coupled with the Forward Laplacian method, obtains accurate energy estimation while significantly reducing the computational cost of model training. Given these promising results, we further explore whether our approach can learn a more useful quantity—the relative energy—across different practical scenarios, including the barrier of chemical reactions, the ionization energy of transition metals, and the noncovalent interaction between molecules. The results demonstrate, for the first time, that the relative energies obtained using NN-VMC methods align with those

obtained using gold-standard computational methods and experimental results, suggesting a great potential of using deep learning to solve quantum mechanical systems.

2 Results

2.1 Forward Laplacian Framework

The most time-consuming part of NN-VMC is the calculation of the Laplacian, i.e., the divergence of the gradient of the network’s output with respect to the coordinates of electrons. In modern deep learning toolkits, one of the most commonly used methods for obtaining the Laplacian is to first compute the Hessian matrix with the **AutoDiff** package and then take its trace [3–6]. However, deriving the Hessian matrix to compute the Laplacian is unnecessary and inefficient, making it far from ideal. We develop a brand-new computational framework, named **Forward Laplacian**, that directly calculates the Laplacian and can significantly improve the computation efficiency of NN-VMC. For the sake of simplicity and without loss of generality, we introduce the implementation and the advantage of Forward Laplacian on the Multi-Layer Perceptron (MLP) network. A detailed analysis of the Forward Laplacian method for general neural networks will be discussed in Section 4.

Let \mathbf{x} denote the input variable (e.g., the electron coordinates) and ϕ denote an arbitrary MLP model. Usually, ϕ can be decomposed into a sequence of linear transformations and non-linear activation functions, i.e., $\phi(x) = F_L \circ F_{L-1} \circ \dots \circ F_0(x)$, where $F_l(\mathbf{h}) = \sigma(W^l \mathbf{h} + b^l)$, $l = 0, \dots, L$. W^l and b^l are learnable parameters and σ is an element-wise activation function. For ease of reference, we denote $\mathbf{h}^{l+1} = F_l(\mathbf{h}^l)$ as the hidden value and $y = F_L(\mathbf{h}^L)$ as the final output. We denote the derivative with respect to variable \mathbf{h} as $\nabla_{\mathbf{h}}$. For simplicity, we use the notation ∇ for the derivative with respect to input and Δ for the Laplacian with respect to input. For a vector-valued function, its Laplacian is derived through applying Δ to each element. To compute $\Delta\phi(\mathbf{x})$, previous method first computes the first-order derivative $\nabla\phi$ through a forward propagation followed by a backward propagation:

$$\begin{aligned} \mathbf{x} \rightarrow \dots \rightarrow \mathbf{h}^l \rightarrow \mathbf{h}^{l+1} \rightarrow \dots \rightarrow y \\ \rightarrow \nabla_{\mathbf{h}^L} y \rightarrow \dots \rightarrow \nabla_{\mathbf{h}^l} y \dots \rightarrow \nabla_{\mathbf{x}} y, \end{aligned} \quad (1)$$

where the chain rule in deriving $\nabla_{\mathbf{h}^l} y$ is given by $\nabla_{\mathbf{h}^l} y = \nabla_{\mathbf{h}^l} F_l(\mathbf{h}^l) \nabla_{\mathbf{h}^{l+1}} y$. The Hessian matrix $\nabla^2\phi$ is calculated through another pass using the following chain rule:

$$\nabla_{\mathbf{h}^{l+1}} = \nabla_{\mathbf{h}^l} \nabla_{\mathbf{h}^l} F_l(\mathbf{h}^l), \quad (2)$$

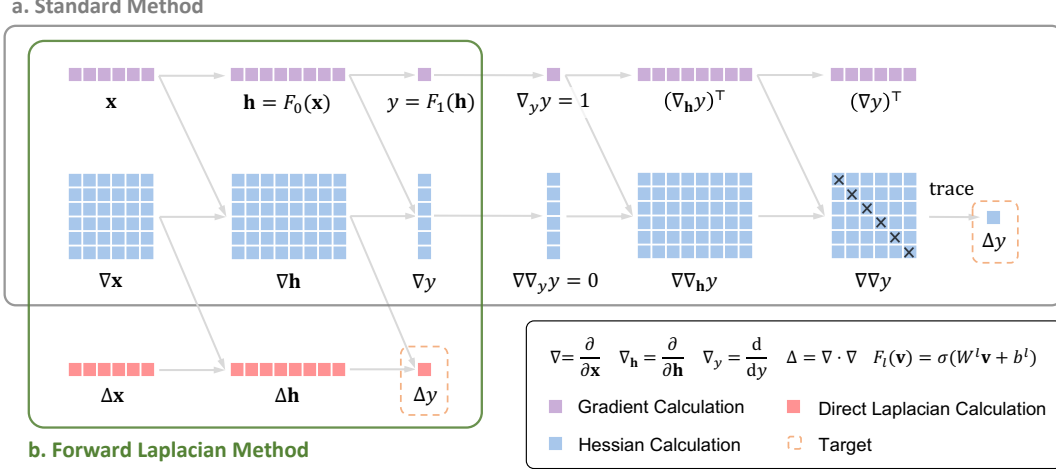


Fig. 1: Illustration of the computation process for Laplacian with the standard method and the proposed Forward Laplacian method. The standard method is presented in the grey box, and our proposed method is presented in the green box. From the figure, we can see that the standard method requires the calculation of Hessian in deriving Laplacian, which is unnecessary and inefficient. In contrast, our method obtains the Laplacian through a carefully crafted forward propagation process, and thus approximately halves the total computational cost.

$$\nabla \nabla_{\mathbf{h}^l} y = \nabla \nabla_{\mathbf{h}^{l+1} y} \nabla_{\mathbf{h}^l} F_l(\mathbf{h}^l)^\top + [(\nabla_{\mathbf{h}^l} \cdot \nabla_{\mathbf{h}^l}) \nabla_{\mathbf{h}^l} F_l(\mathbf{h}^l)] \nabla_{\mathbf{h}^{l+1} y}. \quad (3)$$

The Laplacian is then obtained by taking the trace and the whole computation graph of the method is visualized in Fig. 1a.

Unlike the previous method, we demonstrate that the Laplacian can be calculated efficiently in a direct way. In the forward pass, in each layer l , besides calculating the value of hidden state \mathbf{h}^l , we additionally calculate two terms: the first-order derivative $\nabla_{\mathbf{h}^l}$, as well as the intermediate Laplacian term $\Delta \mathbf{h}^l$.

$$\begin{bmatrix} \mathbf{x} \\ \nabla \mathbf{x} \\ \Delta \mathbf{x} \end{bmatrix} \rightarrow \dots \rightarrow \begin{bmatrix} \mathbf{h}^l \\ \nabla \mathbf{h}^l \\ \Delta \mathbf{h}^l \end{bmatrix} \rightarrow \dots \rightarrow \begin{bmatrix} y \\ \nabla y \\ \Delta y \end{bmatrix}. \quad (4)$$

The key insight in our method is that the calculation of all three terms in layer $l+1$ only requires the term values in layer l , where the chain rule is given by

$$\mathbf{h}^{l+1} = F_l(\mathbf{h}^l) \quad (5)$$

$$\nabla \mathbf{h}^{l+1} = \nabla \mathbf{h}^l \nabla_{\mathbf{h}^l} F_l(\mathbf{h}^l), \quad (6)$$

$$\Delta \mathbf{h}^{l+1} = (\nabla_{\mathbf{h}^l} F_l(\mathbf{h}^l))^\top \Delta \mathbf{h}^l + \text{tr}((\nabla_{\mathbf{h}^l})^\top \nabla_{\mathbf{h}^l} \nabla_{\mathbf{h}^l}^2 F_l(\mathbf{h}^l)). \quad (7)$$

In such a way, all terms are computed iteratively from the first layer, and the value of $\Delta \phi(\mathbf{x})$ will be obtained in the final layer. This method calculates the Laplacian in a single forward pass without computing $\nabla^2 \phi$, thereby avoiding redundant computations.

Additionally, the memory requirements of Forward Laplacian is not significant as the memory that stores intermediate tuple in eq. (4) can be released in the succeeding forward process. The whole computation graph of the proposed method is visualized in Fig. 1b. In Section 4, we provide a detailed analysis of the computational complexity of the Forward Laplacian method, demonstrating that the cost can be approximately halved compared to the previous method. It's important to note that the efficiency is not attributed to any approximation that loses precision but rather to an alternative computational strategy. Hence, our method serves as a more efficient replacement for the previous method in the general setting.

While the Forward Laplacian method offers superior efficiency from a computational point of view, it is crucial yet challenging to integrate it into modern deep learning toolkits and make it compatible with existing frameworks, as the entire training algorithm still heavily relies on many other `AutoDiff` functionalities, e.g., the backward gradient calculation for the network parameters. We implement the Forward Laplacian method in `JAX` [7], a greatly flexible and efficient open-sourced toolkit developed by Google. We carefully overload all the related functions such that when the input of $f(\mathbf{x})$ is a tuple $(\mathbf{x}, \nabla \mathbf{x}, \Delta \mathbf{x})$, the output will automatically become $(f(\mathbf{x}), \nabla f(\mathbf{x}), \Delta f(\mathbf{x}))$. Additionally, for a wide range of elementary operations used in the NN-VMC methods, we manually

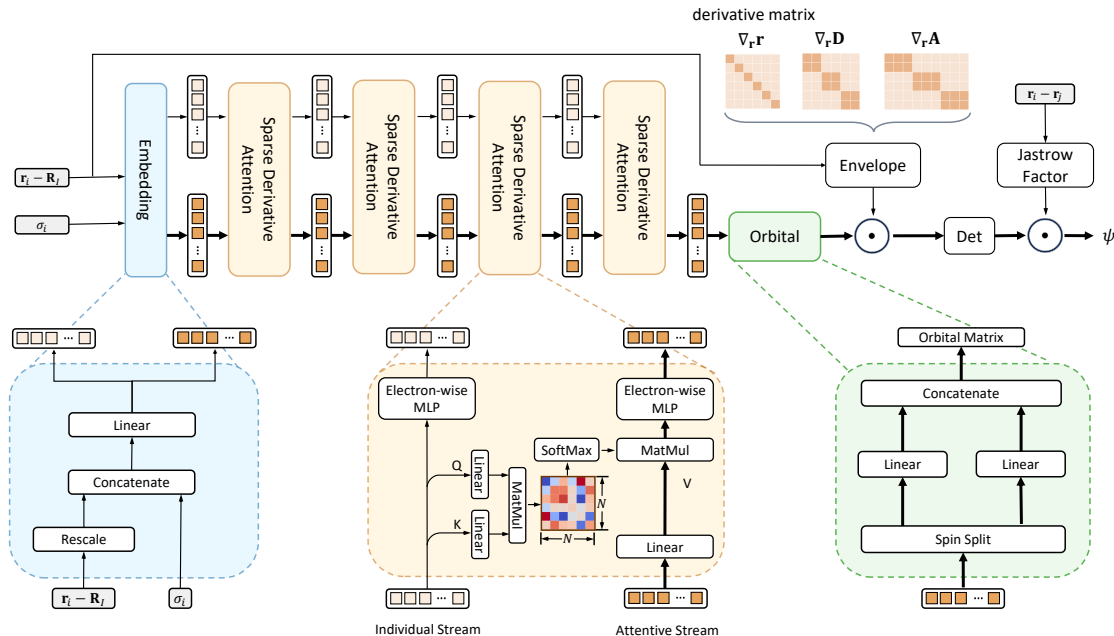


Fig. 2: The LapNet Architecture. The blue block represents the embedding layer, the yellow block represents the sparse derivative attention block, and the green block represents the orbital mapping. The top right part illustrates the derivative sparsity in the envelope function. \mathbf{r} is the input electron position, \mathbf{D} , \mathbf{A} are intermediate matrices. The dark color represents non-zero elements and the light color represents zero elements. The derivative matrices are structurally sparse, thus we can reduce the cost of storing and operating these matrices. A detailed explanation of each block will be shown in Section 4.3.

define their forward propagation rules (e.g., eq. (7)) and optimized their efficiency.

2.2 Accelerating NN-VMC using the Forward Laplacian Framework

In the previous subsection, we introduce a new computational framework that can accelerate the calculation of Laplacian in general settings. In this subsection, we demonstrate that using the proposed framework, we can achieve an even more substantial acceleration rate for some specific classes of neural networks, such as NN-VMC ansatz.

One of the key designs in Forward Laplacian is using forward propagation only. When we applied Forward Laplacian to an NN-VMC ansatz, we found that many intermediate outputs along the propagation naturally exhibit sparsity and can be further optimized to a considerable extent. For example, the *envelope function* (refer to Fig. 2) of any NN-VMC ansatz guarantees that the wavefunction decays exponentially as

electrons move away from atoms. It sequentially computes the relative distance matrix \mathbf{D} between electrons and nuclei, and the exponentially decaying feature matrix \mathbf{A} . Mathematically, $\nabla_{\mathbf{r}}\mathbf{r}$, $\nabla_{\mathbf{r}}\mathbf{D}$, $\nabla_{\mathbf{r}}\mathbf{A}$ are all block-diagonal, where \mathbf{r} denotes the electron positions. Matrix operations can be optimized by leveraging this sparse property. We optimize the Forward Laplacian method to preserve only the non-zero elements and remove others, resulting in an $\mathcal{O}(N)$ efficiency gain in both memory and computation, where N is the number of electrons. The improvement can be applied to various components beyond the envelope function, including the Hartree-Fock function and the Jastrow factor [8]. Remarkably, this technique is only applicable to our framework, as the intermediate variables (e.g., $\nabla_{\mathbf{h}^i}y$) in the standard approach are not sparse.

We then design a new neural network ansatz, namely the **LapNet**, which increases the sparsity during the forward process in Forward Laplacian while maintaining excellent performance compared to other NN-VMC architectures. We illustrate the structure of

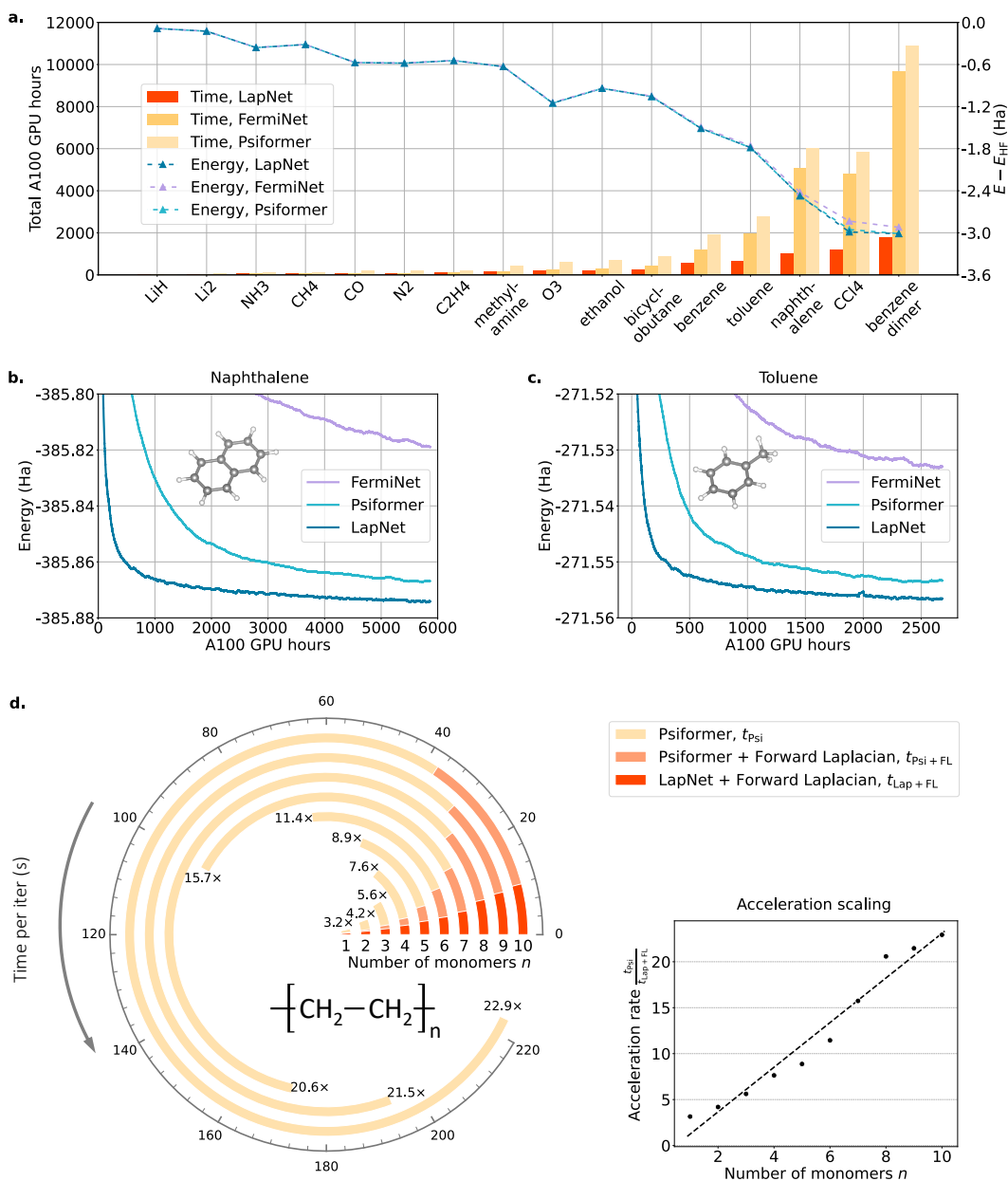


Fig. 3: Efficiency and performance comparison of different NN-VMC methods. **a**, Total training time and energy of LapNet, FermiNet, and Psiformer for 200,000 iterations. The FermiNet and Psiformer results are from [6]. See Supplementary Table 6 for a detailed energy comparison. **b**, **c**, LapNet’s training curve on naphthalene and toluene, compared against the curve of Psiformer and FermiNet. **d**, To investigate the scaling effect of the computational cost with system size, we measure the per-iteration time of different models on Polyethylene systems with varying molecule numbers. We study three models for each system, Psiformer, Psiformer with Forward Laplacian, and LapNet. The speed-up rate of LapNet compared to the original Psiformer is presented at the endpoint of each bar. We also illustrate the dependency between the speed-up rate and the system size on the right side, and the results suggest an almost linear relationship between the acceleration rate and the size of the system.

LapNet in Fig. (2). LapNet incorporates general attention modules, a popular component used in numerous powerful models such as GPT [9] and AlphaFold2 [10]. We develop a *sparse derivative attention* (SDA) block, which is functionally similar to the standard attention block while inherently introducing additional sparsity to the derivative matrices, thereby achieving better efficiency through the Forward Laplacian method. Extensive evaluations in Section 2.3 demonstrate the efficiency and performance of LapNet.

2.3 Efficiency and Performance

In this subsection, we demonstrate that the combination of Forward Laplacian and LapNet achieves state-of-the-art energy results while reducing the computational cost by up to 20 times. We first benchmark LapNet against FermiNet [3] and the recently introduced Psiformer [6], an attention-based neural network ansatz that has shown state-of-the-art performance. The architecture hyperparameters can be found in Supplementary Table 1. Second, we study the runtime scaling law of different methods on polyethylene systems $(C_2H_4)_n$ over different n . Throughout this section, we evaluate the performance of trained models using absolute energy. For baseline approaches, we directly use the open-sourced implementation [11] to measure the corresponding runtime. More details on network training and energy evaluation are discussed in Section 4.

We first calculate the absolute energy on 16 molecular systems with electron numbers ranging from 4 to 84 with 200,000 training iterations. The total training time and energy results of all methods are presented in Fig. 3a. Both LapNet and Psiformer consistently produce lower, namely better, absolute energy than FermiNet across all systems. When compared to Psiformer, the energy results of LapNet either align closely with those of Psiformer within chemical accuracy, or outperform them in the case of certain larger molecules such as CCl_4 . This suggests that LapNet has state-of-the-art capacity for approximating the ground state wavefunction. Regarding the total training time, it is clear from Fig. 3a that LapNet incurs significantly lower costs compared to the baselines. We provide a detailed examination of training curves on naphthalene and toluene in Fig. 3b and Fig. 3c. In both figures, the x -axis indicates the training time instead of the number of iterations, and the y -axis indicates the estimated energy. It is evident that our LapNet converges faster and achieves better accuracy compared to the baselines. This is because LapNet can run for more iterations within the same training period, made possible by the efficient Laplacian calculation in Forward Laplacian, leading to improved accuracy.

To better understand the efficiency enhancements, we investigate the per-iteration computational cost of different models using the polyethylene systems $(C_2H_4)_n$ as an example and set n ranging from 1 to 10. We mainly study three models, one LapNet and two Psiformers. For one of the Psiformers, we use the Forward Laplacian method with sparse derivative matrix optimization, and for the other one, we use the original implementation. The computational cost and speed-up rate of all the models are shown in Fig. 3d. It can be seen from the figure, the Forward Laplacian method can accelerate the Psiformer by 2.6 times when $n = 1$, and 5.9 times when n increases to 10. This observation is consistent with our analysis in Section 2.2 that when the system size grows, the speed-up rate of using the Forward Laplacian method will be more significant. The combination of Forward Laplacian and LapNet generates a speed-up rate exceeding 20 when compared to Psiformer without Forward Laplacian, with $n = 10$. This demonstrates the significant potential of our framework for larger systems. In addition, when comparing the computational cost of Psiformer and LapNet, with Forward Laplacian applied to both, the speed-up rate of LapNet is 2 to 3, which showcases the efficiency improvement of the proposed sparse derivative attention block.

2.4 Pushing the Limits of Relative Energy

In quantum chemistry, relative energy holds greater significance than absolute energy in addressing practical problems. For example, the ionization energy reflects the electron affinity of molecules, the barrier height controls the kinetics of chemical reactions, and the binding energy determines the stability of chemical complexes, to name just a few. Unfortunately, due to the huge computational cost, previous NN-VMC research mainly focused on the absolute energy of small systems, resulting in a lack of comprehensive evaluation pertaining to relative energy. Obtaining accurate relative energy is especially difficult, as the energy scale for relative energy is typically hundreds or thousands of times smaller than that of absolute energy. It is worth noting that although examples of relative energy calculations were reported and discussed in several NN-VMC studies, accurate calculations were only possible for rather small systems and extrapolation techniques were further employed to reduce the error [15, 16]. In this paper, we comprehensively evaluate the relative energy in more challenging and practical systems, thanks to the efficiency improvement brought by Forward Laplacian and LapNet. Specifically, we calculate the ionization potential of 5 metal atoms, reaction barrier heights

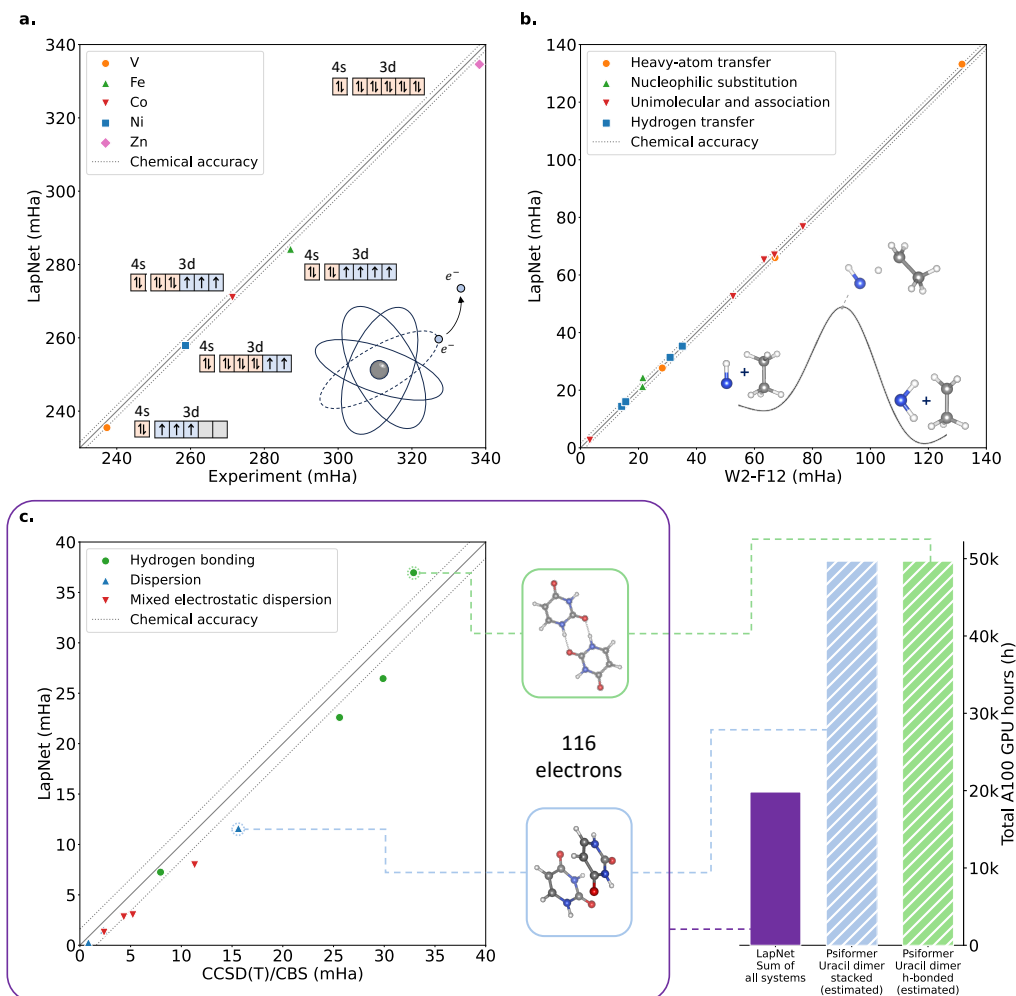


Fig. 4: Relative energy estimation using LapNet. **a.** Estimated ionization potentials of 5 third-row transition metals, compared against experimental results [12]. We also show the 4s and 3d orbital occupations of our calculated ground state next to the symbol for each atom. **b.** Estimated barrier heights of 3 heavy-atom transfer, 2 nucleophilic substitution, 5 unimolecular association, and 4 hydrogen transfer reactions are plotted (see Supplementary Table 4 for details), and W2-F12 data from [13] are used as reference. **c.** Left: Interaction energies of 4 hydrogen-bonding interaction systems, 3 dispersion interaction systems, and 4 mixed electrostatic dispersion interaction systems (see Supplementary Table 5 for details). We take CCSD(T)/CBS results from [14] for comparison. Right: Comparison between the total A100 GPU hours of training all the systems using our method and the estimated A100 GPU hours of training 2 largest systems using Psiformer. All the energy data is given in the Supplementary Table 7, 8, 9.

of 14 reactions, and noncovalent dissociation energy for 11 systems. We compare LapNet with established benchmarks, aiming to better understand the strengths and limitations of the NN-VMC framework.

The ionization potential of an atom can be accurately measured [17–20] through experiments and are widely used to benchmark the *ab initio* calculation methods. We run LapNet to evaluate the ionization potential of five third-row transition metal atoms, namely vanadium (V), iron (Fe), cobalt (Co), nickel (Ni), and zinc (Zn). We train LapNet separately on atoms and the corresponding ions, compute the energy difference as the reported ionization potentials, and compare with the experimental value where the relativistic effects are removed. As shown in Fig. 4a, LapNet can accurately estimate the ionization potentials and achieve chemical accuracy for three out of five systems (V, Co, Ni), and the errors on Fe, Zn are relatively larger (2.9 mHa and 3.7 mHa, respectively). To further study the electronic structure of these transition metals, we calculate the orbital occupations of our wavefunction in outer 4s and 3d shells, as shown in Fig. 4a. The calculated orbital occupations align perfectly with experimental observation, illustrating that our LapNet-based wavefunction is capable of not only producing accurate energy results but also encoding the correct information about the electronic structure.

The barrier height represents the energy difference between the transition state and reactants, determining the minimum energy to activate a chemical reaction and the affecting reaction rate. Therefore, accurate prediction of the barrier is crucial for catalyst design [21]. However, popular *ab initio* methods such as density functional theory (DFT) and CCSD(T) struggle to accurately describe transition states because chemical bonds are partially broken and formed during chemical reactions. In this regard, we have chosen 14 distinct barrier heights from the BH76 dataset [13] encompassing various reaction types such as hydrogen transfer, heavy atom transfer, nucleophilic substitution, and unimolecular association reactions. We use the W2-F12 level of theory [22] in [13] as references. As shown in Fig. 4b, LapNet achieves chemical accuracy for 12 out of 14 reactions, where the average difference is only 0.7 mHa. These results demonstrate that LapNet can accurately estimate the barrier heights.

Non-covalent interactions are critical for maintaining the structure of large chemical and biological molecules. Due to the relatively large contribution of dynamic correlations, standard quantum chemistry methods may face difficulties [23]. To further demonstrate the powerfulness of LapNet, we train LapNet on 11 systems selected from the S22 noncovalent interaction dataset [24], where the largest contains 116

electrons. The selected data encompasses all types of noncovalent interactions in S22, including hydrogen bonding interactions, dispersion interactions, and mixed electrostatic dispersion interactions. To estimate the binding energy of a noncovalent system, we follow the calculation setting in [15] and calculate the energy difference between the dissociated state and the equilibrium state. As shown in Fig. 4c, the average difference over 11 systems is within 2.2 mHa compared to the CCSD(T) benchmark, and LapNet achieves chemical accuracy for 5 out of 11 systems. Our superior efficiency allows for the fine-grained investigation of large systems with more than a hundred electrons and sheds light on future improvement of NN-VMC methods. For instance, across the analysis of 11 systems, we notice that LapNet typically overestimates the energies of equilibrium states since their electron structures are more complex than that of dissociated states. Inspired by this observation, future NN-VMC methods should focus more on expressing the electron structures of equilibrium states to achieve better calculation results.

We would like to highlight that this comprehensive investigation into relative energies would not be possible without the help of Forward Laplacian and LapNet. Prior to our work, the largest molecular system analyzed by previous NN-VMC methods was the benzene dimer system with 84 electrons. However, their training requires more than 10,000 A100 GPU hours, while ours requires only 1,800 GPU hours, giving a 6 times acceleration. In addition, LapNet is able to estimate even larger systems, such as the uracil dimer with 116 electrons. On the right side of Fig. 4c, we present the GPU hours to compute all the 11 systems with LapNet and compare it with the computational cost of Psiformer to finish the two largest systems, uracil dimer stack and uracil dimer h-bonded. Due to the huge computational cost, we only estimate the GPU hours of these two training process using `per_iteration.cost × num_iteration`, where `num_iteration` is set to 200,000, following all previous works [3, 6]. It can be clearly seen that calculating all the systems using our method is even faster than calculating one system using the original Psiformer.

In summary, we demonstrate the potential of LapNet to estimate different types of relative energies. The significantly improved efficiency allows a more comprehensive study of a wide range of large chemical systems, which is beneficial for the development of NN-VMC methods and the field of computational quantum chemistry.

3 Discussion

NN-VMC methods have been used for ground-state energy estimation in a wide range of applications, including molecular systems [3–6, 25–28], solid systems [29, 30], and homogeneous electron gas [31–33]. The approach has been extended to compute other important quantities, such as excitation energy [16], inter-atomic force [34] and electric polarization [35]. Recently, several works further combined NN-VMC methods with other classical methods, such as Effective Core Potential [36] and Diffusion Monte Carlo [15, 37]. Refs. [38–42] learn universal representations of wavefunctions on multiple systems to enable transfer learning to unseen system configurations. Notably, in all of these works, the Laplacian calculation with neural networks is indispensable. Our proposed Forward Laplacian offers advantages for all the aforementioned methods and can be integrated with all existing NN-VMC packages [11, 43, 44].

Although our proposed approach yields relative energies that align closely with the gold standard or experimental results in most cases, there are instances where discrepancies persist between our results and ground truth. Our hypothesis for this inconsistency is that existing NN-VMC methods inadequately incorporate all critical chemical and physical knowledge. For instance, the error cancellation property, which is crucial for obtaining accurate relative energies in gold-standard methods like CCSD(T), is not inherently encoded in the NN-VMC ansatz or prevailing training strategies. We believe encoding proper chemical and physical knowledge into neural networks will be vital in advancing NN-VMC techniques in the future.

Our principal objective is to tackle the computational bottleneck associated with the calculation of the Laplacian in the NN-VMC methods. However, the prospective utilization of our Forward Laplacian approach could extend to diverse scenarios outside the realm of quantum mechanics. As shown in the Method section, the Forward Laplacian method can replace the previous method with improved efficiency when calculating Laplacian associated with any neural network. Therefore, it can accelerate the training of other neural network-based solvers of partial differential equations [45–47], such as heat diffusion equations and Navier-Stokes equations.

4 Methods

4.1 Wavefunction Optimization

For a molecular system with N electrons and M nuclei, we consider the time-independent Schrödinger

equation under the Born-Oppenheimer approximation:

$$\hat{H}\psi(\mathbf{x}_1, \dots, \mathbf{x}_N) = E\psi(\mathbf{x}_1, \dots, \mathbf{x}_N), \quad (8)$$

$$\hat{H} = -\frac{1}{2} \sum_i \Delta_i + \sum_{i>j} \frac{1}{|\mathbf{r}_i - \mathbf{r}_j|} \quad (9)$$

$$- \sum_{I} \frac{Z_I}{|\mathbf{r}_i - \mathbf{R}_I|} + \sum_{I>J} \frac{Z_I Z_J}{|\mathbf{R}_I - \mathbf{R}_J|}, \quad (10)$$

where $\mathbf{x}_i = \{\mathbf{r}_i, \sigma_i\}$ is the coordinate of electron i . $\mathbf{r}_i \in \mathbb{R}^3$ is the position of the i -th electron and $\sigma_i \in \{1, -1\}$ is the spin coordinate. Z_I is the charge of the I -th nucleus and \mathbf{R}_I is the corresponding position. Δ_i is the Laplacian w.r.t. \mathbf{r}_i . For ease of reference, we denote $(\mathbf{x}_1, \mathbf{x}_2, \dots, \mathbf{x}_N)$ as \mathbf{x} .

The wavefunction of a multi-electron system should be antisymmetric under the exchange of any electron’s coordinates of the same spin, i.e.,

$$\psi(\dots, \mathbf{x}_i, \dots, \mathbf{x}_j) = -\psi(\dots, \mathbf{x}_j, \dots, \mathbf{x}_i). \quad (11)$$

Following previous methods, we leverage the form of Slater-Jastrow-Backflow ansatz to satisfy this condition:

$$\psi_\theta(\mathbf{x}) = e^{J_\theta(\mathbf{x})} \sum_{k=1}^K \det[\Phi_\theta^k(\mathbf{x})], \quad (12)$$

where $J_\theta(\mathbf{x})$ is the Jastrow factor and $\Phi_\theta^k(\mathbf{x})$ is a permutation-equivariant neural network. The output of this network is used as the input for the k -th Slater determinant.

Following [3], the training of NN-VMC is divided into two phases. The first is the pre-training phase in which $\Phi_\theta^k(\mathbf{x})$ is updated to match the Hartree-Fock orbitals. The second is the VMC training phase where we optimize the parameters to minimize the total energy of the wavefunction defined below.

$$\begin{aligned} \mathcal{L}_\theta &= \frac{\langle \psi_\theta | \hat{H} | \psi_\theta \rangle}{\langle \psi_\theta | \psi_\theta \rangle} = \frac{\int \psi_\theta^*(\mathbf{x}) \hat{H} \psi_\theta(\mathbf{x}) d\mathbf{x}}{\int \psi_\theta^*(\mathbf{x}) \psi_\theta(\mathbf{x}) d\mathbf{x}} \\ &= \int p(\mathbf{x}) E_L(\mathbf{x}) d\mathbf{x}. \end{aligned} \quad (13)$$

$E_L(\mathbf{x}) = \psi_\theta^{-1}(\mathbf{x}) \hat{H} \psi_\theta(\mathbf{x})$ is known as the local energy, and $p(\mathbf{x}) = \frac{\psi_\theta^*(\mathbf{x}) \psi_\theta(\mathbf{x})}{\langle \psi_\theta | \psi_\theta \rangle}$. We use gradient descent to optimize the parameters, where the unbiased estimate of θ ’s gradient is given by:

$$\nabla_\theta \mathcal{L}_\theta = 2\mathbb{E}_{p(\mathbf{x})}[(E_L - \mathbb{E}_{p(\mathbf{x})}[E_L]) \nabla_\theta \log |\psi_\theta|]. \quad (14)$$

The loss function and the gradient are estimated using the Metropolis-Hastings algorithm, one of the most popular Markov Chain Monte Carlo (MCMC) methods. To make the initial electron distribution closer to the target distribution, we assign each electron to a nucleus according to the Mulliken population analysis [48] results within the Hartree-Fock method. Initial electron positions are then sampled from Gaussian distributions centered around the corresponding

atom. The convergence of the wavefunction to the ground state is achieved through iterative sampling and updates of parameters during training. For evaluation, we follow [3] and run MCMC steps without updating the network parameters to sample batches of workers and compute their local energy. The total energy and associated standard error are determined by reblocking analysis.

In practice, the accuracy of a learned model can be significantly influenced by the quality of its pre-training phase. The Hartree-Fock solution may be inaccurate when the electron structure is complex, such as in transition metals, which may result in an inaccurate initialization of the neural network during a prolonged pre-training phase. To mitigate this issue, we use a short pre-training phase alongside a moderate basis set for the Hartree-Fock method. This strategy results in improved performance on complex systems like CCl₄. All training hyperparameters are listed in Supplementary Table 2 and 3.

4.2 Forward Laplacian Method for General Neural Networks

In this subsection, we provide a detailed explanation of how the Forward Laplacian method accelerates the calculation of Laplacian for general neural networks. The computation graph serves as the descriptive language of deep learning models across various deep learning toolkits, including PyTorch [49], TensorFlow [50], and Jax [7]. Therefore, we can narrow our focus to investigating the performance of the proposed method in a specific computation graph.

In a computation graph \mathcal{G} , the edges represent function arguments, and nodes represent operations or variables. Note that \mathcal{G} is always a directed acyclic graph. We use $\{\mathbf{v}^{-1}, \dots, \mathbf{v}^{-N}\}$ to represent the external nodes of \mathcal{G} (i.e., the input of the neural network), and use $\{\mathbf{v}^0, \dots, \mathbf{v}^M\}$ to represent the internal nodes, sorted in topological orders. \mathbf{v}^M serves as the network output ϕ . We use the abbreviation $i \rightarrow j$ if there is a directed edge from \mathbf{v}^i to \mathbf{v}^j in \mathcal{G} . Furthermore, we denote operations as F , e.g., $\mathbf{v}^j = F_j(\{\mathbf{v}^i : i \rightarrow j\})$ for all $j \geq 0$.

We first show that the Forward Laplacian method can be applied to general neural networks, such as FermiNet, Psiformer, and LapNet. Similar to Section 2.1, along the computation graph, we compute the tuple $(v_j, \nabla v_j, \Delta v_j)$ for each node. To be specific, the tuple associated with node j is derived through chain rules[51]:

$$\mathbf{v}^j = F_j(\{\mathbf{v}^i : i \rightarrow j\}) \quad (15)$$

$$\nabla \mathbf{v}^j = \sum_{i:i \rightarrow j} \frac{\partial F_j}{\partial \mathbf{v}^i} \nabla \mathbf{v}^i \quad (16)$$

$$\Delta \mathbf{v}^j = \sum_{\substack{i,l \\ i \rightarrow j, l \rightarrow j}} \frac{\partial^2 F_j}{\partial \mathbf{v}^i \partial \mathbf{v}^l} \nabla \mathbf{v}^i \cdot \nabla \mathbf{v}^l + \sum_{i:i \rightarrow j} \frac{\partial F_j}{\partial \mathbf{v}^i} \Delta \mathbf{v}^i \quad (17)$$

Note that eqs. (15) - (17) only rely on tuples associated with parent nodes of j . Therefore, we can sequentially apply eqs. (15) - (17) to nodes of any computational graph in topological orders, and finally get the Laplacian in the output node.

We then analyze the speed-up rate of the Forward Laplacian method compared to the previous method. The previous method obtains $\Delta \phi(\mathbf{x})$ through computing the Hessian matrix. It first performs forward propagation to obtain the value of each variable \mathbf{v}^j . Next, a standard backward process is employed by creating a new computation graph $\hat{\mathcal{G}}$ where node $\hat{\mathbf{v}}^i \in \hat{\mathcal{G}}$ represents the operation to calculate $\frac{\partial \phi}{\partial \mathbf{v}^i}$, $i = M, \dots, -N$. The associated computations are

$$\frac{\partial \phi}{\partial \mathbf{v}^i} = \sum_{j:i \rightarrow j} \frac{\partial F_j}{\partial \mathbf{v}^i} \frac{\partial \phi}{\partial \mathbf{v}^j}, \quad i = M - 1, \dots, -N. \quad (18)$$

The Hessian matrix is then obtained through the following forward-mode Jacobian calculation along \mathcal{G} and $\hat{\mathcal{G}}$, respectively:

$$\begin{aligned} \nabla \mathbf{v}^i &= \sum_{j:j \rightarrow i} \frac{\partial F_j}{\partial \mathbf{v}^i} \nabla \mathbf{v}^j \quad (19) \\ \nabla \frac{\partial \phi}{\partial \mathbf{v}^i} &= \sum_{\substack{j,l \\ i \rightarrow j, l \rightarrow j}} \frac{\partial^2 F_j}{\partial \mathbf{v}^l \partial \mathbf{v}^i} \frac{\partial \phi}{\partial \mathbf{v}^j} \nabla \mathbf{v}^l + \sum_{j:i \rightarrow j} \frac{\partial F_j}{\partial \mathbf{v}^i} \nabla \frac{\partial \phi}{\partial \mathbf{v}^j}, \quad (20) \end{aligned}$$

where we always use ∇ to denote $\nabla_{\mathbf{x}}$ for simplicity.

The bottleneck of Hessian computation comes from eq. (19) and eq. (20). eq. (19) takes $N|E|$ floating point operations (FLOPs) if we only count multiplications, where E denotes the set of edges in \mathcal{G} . For eq. (20), the second term also takes $N|E|$ FLOPs. To calculate the computational cost of the first term in eq. (20), we first introduce two notations, T and R , which are both sets of ordered tuples:

$$\begin{aligned} T &= \{(i, l, j) | i \rightarrow j, l \rightarrow j, \frac{\partial^2 F_j}{\partial \mathbf{v}^i \partial \mathbf{v}^l} \neq 0\}, \quad (21) \\ R &= \{(i, l) | \exists j \text{ s.t. } (i, l, j) \in T\}. \end{aligned}$$

The previous method sums over j first to obtain $\sum_{j:i \rightarrow j, l \rightarrow j} \frac{\partial^2 F_j}{\partial \mathbf{v}^l \partial \mathbf{v}^i} \frac{\partial \phi}{\partial \mathbf{v}^j}$ for all $(i, l) \in R$, and then sums over l . It can be shown that the total computation cost of this term is $0.5|T| + N|R|$ by exploiting the symmetry of the Hessian matrix. Thus, the total FLOPs for the previous method is about $N(|R| + 2|E|) + 0.5|T|$.

For the proposed Forward Laplacian method, we perform forward propagation along \mathcal{G} to obtain $\phi(\mathbf{x})$, $\nabla\phi(\mathbf{x})$ and $\Delta\phi(\mathbf{x})$. The second term $\nabla\phi(\mathbf{x})$ is calculated along \mathcal{G} according to eq. (16). The third term, i.e., the Laplacian, is calculated along \mathcal{G} according to eq. (17).

The computational cost of the Forward Laplacian method is dominated by eq. (16) and eq. (17). As previously discussed, eq. (16) takes $N|E|$ FLOPs. For the first term in eq. (17), we decompose its calculation into two steps. First, we compute $\{\nabla\mathbf{v}^j \cdot \nabla\mathbf{v}^l\}_{j \leq l, (j,l) \in R}$, which takes $0.5N|R|$ FLOPs in total. Next, following the topological order of \mathcal{G} , we sum over $j \leq l$ for each i , deriving the first term in $\Delta\mathbf{v}^i$. By leveraging the symmetry of the Hessian matrix and Gram matrix, we reduce this computation by a factor of 2, which is $0.5|T|$ FLOPs. The computational cost of the second term is negligible compared with the first term since $\Delta\mathbf{v}^j$ is a scalar. Summing the computational cost of all the terms, we have that the Forward Laplacian method uses $0.5N(|R| + 2|E|) + 0.5|T|$. In practice, a large percentage of operations are linear transformations, and for any linear operation F_j , $\frac{\partial^2 F_j}{\partial\mathbf{v}^i \partial\mathbf{v}^l} = 0$ for any $i \rightarrow j, l \rightarrow j$. This means the value $|T|$ is much smaller than $N|R|$ and $N|E|$. Thus, our method is about two times faster than the previous method for computing Laplacian.

We implement the Forward Laplacian method in `Jax`[7]. We overload a large number of frequently used operations such that if the input of $f(\mathbf{x})$ is a Laplacian tuple $(\mathbf{x}, \nabla\mathbf{x}, \Delta\mathbf{x})$, the output will automatically become another Laplacian tuple $(f(\mathbf{x}), \nabla f(\mathbf{x}), \Delta f(\mathbf{x}))$. This process is implemented via `Python` decorator, which can make our implementation compatible with existing operations. To achieve further acceleration, we manually define the forward propagation rules for a wide range of operations used in NN-VMC methods and optimize their efficiency in computing the Laplacian tuple. Specifically, we mainly optimize two classes of operations, namely **element-wise operations**, **linear operations**, and several frequently used non-linear operations.

Element-wise operations apply a scalar function to each element of the input array and output an array with the same shape. Many operations in neural networks are element-wise, such as activation and exponential functions. The Jacobian matrix is always diagonal for these operations, and there is no need to calculate non-diagonal elements. We implement a customized framework for element-wise functions to avoid unnecessary calculations, thus speeding up the Laplacian computation. An operation f is linear if $f(\mathbf{x} + \mathbf{y}) = f(\mathbf{x}) + f(\mathbf{y})$. Here \mathbf{x}, \mathbf{y} are arrays. For example, `reshape`, `concatenate`, `sum` are all linear. It can be proved that for linear operations, we have

$\nabla f(\mathbf{x}) = f(\nabla\mathbf{x})$. Based on this, we can compute $\nabla f(\mathbf{x}), \Delta f(\mathbf{x})$ by directly ‘‘applying’’ f on $\nabla\mathbf{x}, \Delta\mathbf{x}$, thus avoiding second-order calculations. For operations that are not mentioned above, but are commonly used such as `matmul`, `slogdet`, `softmax`, we manually customize the computation rules case-by-case as they significantly differ from one another.

4.3 LapNet Ansatz

To better leverage the benefits of the Forward Laplacian method, we develop a neural network architecture, called LapNet. This architecture facilitates a significant faster Laplacian calculation [52] thus improves the training speed further without sacrificing any accuracy compared to the previous state-of-the-art approach [6]. The overall architecture of LapNet is illustrated in Fig. 2.

We use the relative position of electron-nuclei pairs $\mathbf{r}_i - \mathbf{R}_I$ and the electron spins σ_i as the input features. Following [6], a norm-rescaled function `Rescale` : $\mathbb{R}^3 \rightarrow \mathbb{R}^4$ is applied to each electron-nuclei pair:

$$\mathbf{e}_{iI} = \text{Rescale}(\mathbf{r}_i - \mathbf{R}_I), \quad (22)$$

where each output dimension of `Rescale`(\mathbf{z}) is given by:

$$\begin{aligned} \text{Rescale}_1(\mathbf{z}) &= \ln(1 + |\mathbf{z}|)\hat{\mathbf{z}}_1 \\ \text{Rescale}_2(\mathbf{z}) &= \ln(1 + |\mathbf{z}|)\hat{\mathbf{z}}_2 \\ \text{Rescale}_3(\mathbf{z}) &= \ln(1 + |\mathbf{z}|)\hat{\mathbf{z}}_3 \\ \text{Rescale}_4(\mathbf{z}) &= \ln(1 + |\mathbf{z}|). \end{aligned} \quad (23)$$

$|\cdot|$ refers to the L_2 norm and $\hat{\mathbf{z}} = \mathbf{z}/|\mathbf{z}|$ is the directional vector of \mathbf{z} , the subscripts refer to the index of coordinates. Then, $\{\mathbf{e}_{iI}\}_{I=1}^M$ is concatenated with σ_i to form the feature set for electron i :

$$\mathbf{d}_i = \text{Concat}(\{\mathbf{e}_{iI}\}_{I=1}^M, \sigma_i). \quad (24)$$

\mathbf{d}_i is then projected via a linear layer into two terms $\mathbf{h}_i^0, \mathbf{g}_i^0$, which will be further fed into the LapNet. We denote $\mathbf{h}^0 = (\mathbf{h}_1^0, \dots, \mathbf{h}_i^0, \dots, \mathbf{h}_N^0)$ and $\mathbf{g}^0 = (\mathbf{g}_1^0, \dots, \mathbf{g}_i^0, \dots, \mathbf{g}_N^0)$ for ease of reference.

The main building block of LapNet is the stacked Sparse Derivative Attention (SDA) module. The l -th SDA module takes $\mathbf{h}^l, \mathbf{g}^l$ as input and outputs $\mathbf{h}^{l+1}, \mathbf{g}^{l+1}$ through two streams.

\mathbf{g}^l is updated by a stream called the individual stream, where each \mathbf{g}_i^l is updated as below

$$\mathbf{g}_i^{l+1} = \mathbf{g}_i^l + \text{MLP}_{\text{indiv}}^l(\mathbf{g}_i^l). \quad (25)$$

In the individual stream, each electron i independently updates its own features using MLPs with parameter sharing. Since there is no interaction between different electrons in the stream, the derivative matrix $\nabla_{\mathbf{r}}\mathbf{g}^l$ is sparse, i.e., $\nabla_{\mathbf{r}_{i'}}\mathbf{g}_i^l = 0$ when $i \neq i'$. As shown in Section 2.2, this sparsity leads to acceleration with the Forward Laplacian method.

\mathbf{h}^l is updated by the other stream called attentive stream, where the features of different electrons interact with each other through attention. In the attention, we use individual-stream-produced \mathbf{g}^l as queries and keys, and use attention-stream-produced \mathbf{h}^l as Values with different linear projection layers.

$$\mathbf{q}_i = W_Q^l \mathbf{g}_i^l, \mathbf{k}_i = W_K^l \mathbf{g}_i^l, \mathbf{v}_i = W_V^l \mathbf{h}_i^l, \quad (26)$$

Matrices W_Q^l , W_K^l and W_V^l are learnable parameters of the l -th block. We use normalized dot products to calculate weights assigned to different value terms and the update of \mathbf{h}^l is given by

$$\bar{\mathbf{h}}_i^{l+1} = \mathbf{h}_i^l + \sum_j \alpha_{ij} \mathbf{v}_j \quad (27)$$

$$\mathbf{h}_i^{l+1} = \bar{\mathbf{h}}_i^{l+1} + \text{MLP}_{\text{attn}}^l(\bar{\mathbf{h}}_i^{l+1}), \quad (28)$$

where

$$\alpha_{ij} = \frac{S_{ij}}{\sum_{j'} S_{ij'}}, S_{ij} = \exp(\mathbf{q}_i^\top \mathbf{k}_j) \quad (29)$$

Note that queries and keys used in the attentive stream are independently updated in the individual stream. Therefore the S_{ij} also exhibit a certain level of derivative sparsity. As a result, this design facilitates efficient computation through our Forward Laplacian method.

After stacking L layers of Sparse Derivative Attention blocks, we use the output of attentive stream \mathbf{h}_i^L to construct the wavefunction. Our wavefunction follows the Slater-Jastrow-Backflow ansatz [53]:

$$\psi_\theta(\mathbf{x}) = e^{J_\theta(\mathbf{x})} \sum_{k=1}^K \det[\Phi_\theta^k(\mathbf{x})]. \quad (30)$$

To construct Φ_θ^k , we first project \mathbf{h}_i^L to \mathbb{R}^N using a spin-dependent linear transformation:

$$\mathbf{o}_i^k = \mathbf{W}_{\sigma_i}^k \mathbf{h}_i^L + \mathbf{b}_{\sigma_i}^k, \quad (31)$$

To ensure the wavefunction approaches zero when the electron moves away from all nuclei, we use the envelope function and multiply it with \mathbf{o}_i^k to obtain $\Phi_\theta^k(\mathbf{x})$:

$$\text{env}_j(\mathbf{x}_i) = \sum_I \pi_{I_j}^{\sigma_i} e^{-|\xi_{I_j}^{\sigma_i}| |\mathbf{r}_i - \mathbf{R}_I|}, \quad (32)$$

$$[\Phi_\theta^k(\mathbf{x})]_{ji} = \text{env}_j(\mathbf{x}_i) [\mathbf{o}_i^k]_j, \quad (33)$$

where $\pi_{I_j}^{\sigma_i}$ and $\xi_{I_j}^{\sigma_i}$ are learnable parameters. In practice, we observed some determinants $\det[\Phi_\theta^k(\mathbf{x})]$ degenerate and we remove those determinants during training. We use a simple form for the Jastrow factor in eq. (30) to satisfy the electron-electron Cusp condition [8]:

$$J_\theta(\mathbf{x}) = \sum_{i < j; \sigma_i = \sigma_j} -\frac{1}{4} \frac{\alpha_{\text{par}}^2}{\alpha_{\text{par}} + |\mathbf{r}_i - \mathbf{r}_j|} + \sum_{i < j; \sigma_i \neq \sigma_j} -\frac{1}{2} \frac{\alpha_{\text{anti}}^2}{\alpha_{\text{anti}} + |\mathbf{r}_i - \mathbf{r}_j|}, \quad (34)$$

where α_{par} and α_{anti} are learnable parameters. Combining with $\det[\Phi_\theta^k(\mathbf{x})]$, the wavefunction is finally computed through eq. (30). As discussed above, the LapNet incorporates more derivative sparsity in many operations related to \mathbf{g}_i^l , \mathbf{q}_i , \mathbf{k}_i and S_{ij} , leading to a significantly speed-up rate compared to previous architectures.

Acknowledgments. We thank Hang Li and ByteDance Research for support and inspiration. We thank David Pfau for his valuable feedback. We thank Bohang Zhang and Haiyang Wang for their helpful suggestion and discussion. Liwei Wang is supported by National Key R&D Program of China (2022ZD0114900) and National Science Foundation of China (NSFC62276005). J.C. acknowledges the National Natural Science Foundation of China for support under Grant No. 92165101.

References

- [1] Needs, R.J., Towler, M.D., Drummond, N.D., López Ríos, P., Trail, J.R.: Variational and diffusion quantum Monte Carlo calculations with the CASINO code. The Journal of Chemical Physics **152**(15), 154106 (2020) <https://doi.org/10.1063/1.5144288>
- [2] Foulkes, W.M.C., Mitras, L., Needs, R.J., Rajagopal, G.: Quantum Monte Carlo simulations of solids. Reviews of Modern Physics **73**(1), 33–83 (2001) <https://doi.org/10.1103/RevModPhys.73.33>
- [3] Pfau, D., Spencer, J.S., G. Matthews, A.G., Foulkes, W.M.C.: Ab-initio solution of the many-electron schrödinger equation with deep neural networks. Physical Review Research **2**, 033429 (2020) <https://doi.org/10.1103/PhysRevResearch.2.033429>
- [4] Spencer, J.S., Pfau, D., Botev, A., Foulkes, W.M.C.: Better, Faster Fermionic Neural Networks. arXiv:2011.07125 (2020)
- [5] Hermann, J., Schätzle, Z., Noé, F.: Deep-neural-network solution of the electronic Schrödinger equation. Nature Chemistry **12**(10), 891–897 (2020)
- [6] Glehn, I., Spencer, J.S., Pfau, D.: A

- self-attention ansatz for ab-initio quantum chemistry. In: The Eleventh International Conference on Learning Representations (2023). <https://openreview.net/forum?id=xveTeHVIF7j>
- [7] Bradbury, J., et al.: JAX: Composable Transformations of Python+NumPy programs. <http://github.com/google/jax>
- [8] Drummond, N.D., Towler, M.D., Needs, R.J.: Jastrow correlation factor for atoms, molecules, and solids. *Physical Review B* **70**, 235119 (2004) <https://doi.org/10.1103/PhysRevB.70.235119>
- [9] Brown, T., Mann, B., Ryder, N., Subbiah, M., Kaplan, J.D., Dhariwal, P., Neelakantan, A., Shyam, P., Sastry, G., Askell, A., Agarwal, S., Herbert-Voss, A., Krueger, G., Henighan, T., Child, R., Ramesh, A., Ziegler, D., Wu, J., Winter, C., Hesse, C., Chen, M., Sigler, E., Litwin, M., Gray, S., Chess, B., Clark, J., Berner, C., McCandlish, S., Radford, A., Sutskever, I., Amodei, D.: Language models are few-shot learners. In: *Advances in Neural Information Processing Systems*, vol. 33, pp. 1877–1901 (2020). https://proceedings.neurips.cc/paper_files/paper/2020/file/1457c0d6bfcb4967418bfb8ac142f64a-Paper.pdf
- [10] Jumper, J., Evans, R., Pritzel, A., Green, T., Figurnov, M., Ronneberger, O., Tunyasuvunakool, K., Bates, R., Žídek, A., Potapenko, A., Bridgland, A., Meyer, C., Kohl, S.A.A., Ballard, A.J., Cowie, A., Romera-Paredes, B., Nikolov, S., Jain, R., Adler, J., Back, T., Petersen, S., Reiman, D., Clancy, E., Zielinski, M., Steinegger, M., Pacholska, M., Berghammer, T., Bodenstein, S., Silver, D., Vinyals, O., Senior, A.W., Kavukcuoglu, K., Kohli, P., Hassabis, D.: Highly accurate protein structure prediction with AlphaFold. *Nature* **596**(7873), 583–589 (2021) <https://doi.org/10.1038/s41586-021-03819-2>
- [11] James S. Spencer, D.P., Contributors, F.: FermiNet. <http://github.com/deepmind/ferminet>
- [12] Balabanov, N.B., Peterson, K.A.: Basis set limit electronic excitation energies, ionization potentials, and electron affinities for the 3d transition metal atoms: Coupled cluster and multireference methods. *The Journal of Chemical Physics* **125**(7), 074110 (2006) <https://doi.org/10.1063/1.2335444>
- [13] Goerigk, L., Hansen, A., Bauer, C., Ehrlich, S., Najibi, A., Grimme, S.: A look at the density functional theory zoo with the advanced gmtkn55 database for general main group thermochemistry, kinetics and noncovalent interactions. *Physical Chemistry Chemical Physics* **19**, 32184–32215 (2017) <https://doi.org/10.1039/C7CP04913G>
- [14] Marshall, M.S., Burns, L.A., Sherrill, C.D.: Basis set convergence of the coupled-cluster correction, $\delta_{MP2}^{CCSD(T)}$: Best practices for benchmarking non-covalent interactions and the attendant revision of the S22, NBC10, HBC6, and HSG databases. *The Journal of Chemical Physics* **135**(19) (2011) <https://doi.org/10.1063/1.3659142>
- [15] Ren, W., Fu, W., Wu, X., Chen, J.: Towards the ground state of molecules via diffusion monte carlo on neural networks. *Nature Communications* **14**(1), 1860 (2023) <https://doi.org/10.1038/s41467-023-37609-3>
- [16] Entwistle, M.T., Schätzle, Z., Erdman, P.A., Hermann, J., Noé, F.: Electronic excited states in deep variational Monte Carlo. *Nature Communications* **14**(1), 274 (2023) <https://doi.org/10.1038/s41467-022-35534-5>
- [17] Sugar, J., Corliss, C.: Atomic energy levels of the iron-period elements: potassium through nickel. *Journal of Physical and Chemical Reference Data* **14**(Suppl. 2), 1 (1985)
- [18] Page, R.H., Gudeman, C.S.: Completing the iron period: double-resonance, fluorescence-dip rydberg spectroscopy and ionization potentials of titanium, vanadium, iron, cobalt, and nickel. *Journal of the Optical Society of America B* **7**(9), 1761–1771 (1990) <https://doi.org/10.1364/JOSAB.7.001761>

- [19] Sohl, J.E., Zhu, Y., Knight, R.D.: Two-color laser photoionization spectroscopy of Ti i: multichannel quantum defect theory analysis and a new ionization potential. *Journal of the Optical Society of America B* **7**(1), 9–14 (1990) <https://doi.org/10.1364/JOSAB.7.000009>
- [20] James, A.M., Kowalczyk, P., Langlois, E., Campbell, M.D., Ogawa, A., Simard, B.: Resonant two photon ionization spectroscopy of the molecules V2, VNb, and Nb2. *The Journal of Chemical Physics* **101**(6), 4485–4495 (1994) <https://doi.org/10.1063/1.468462>
- [21] Spiekermann, K., Pattanaik, L., Green, W.H.: High accuracy barrier heights, enthalpies, and rate coefficients for chemical reactions. *Scientific Data* **9**(1), 417 (2022) <https://doi.org/10.1038/s41597-022-01529-6>
- [22] Karton, A., Martin, J.M.L.: Explicitly correlated Wn theory: W1-F12 and W2-F12. *The Journal of Chemical Physics* **136**(12) (2012) <https://doi.org/10.1063/1.3697678>
- [23] Al-Hamdani, Y.S., Nagy, P.R., Zen, A., Barton, D., Kállay, M., Brandenburg, J.G., Tkatchenko, A.: Interactions between large molecules pose a puzzle for reference quantum mechanical methods. *Nature Communications* **12**(1), 3927 (2021)
- [24] Jurečka, P., Šponer, J., Černý, J., Hobza, P.: Benchmark database of accurate (MP2 and CCSD (T) complete basis set limit) interaction energies of small model complexes, DNA base pairs, and amino acid pairs. *Physical Chemistry Chemical Physics* **8**(17), 1985–1993 (2006)
- [25] Han, J., Zhang, L., E, W.: Solving many-electron schrödinger equation using deep neural networks. *Journal of Computational Physics* **399**, 108929 (2019) <https://doi.org/10.1016/j.jcp.2019.108929>
- [26] Lin, J., Goldshlager, G., Lin, L.: Explicitly antisymmetrized neural network layers for variational monte carlo simulation. *Journal of Computational Physics* **474**, 111765 (2023)
- [27] Abrahamsen, N., Lin, L.: Taming the sign problem of explicitly antisymmetrized neural networks via rough activation functions. *arXiv preprint arXiv:2205.12250* (2022)
- [28] Gerard, L., Scherbela, M., Marquetand, P., Grohs, P.: Gold-standard solutions to the schrödinger equation using deep learning: How much physics do we need? In: Oh, A.H., Agarwal, A., Belgrave, D., Cho, K. (eds.) *Advances in Neural Information Processing Systems* (2022). <https://openreview.net/forum?id=nX-gReQ00T>
- [29] Li, X., Li, Z., Chen, J.: Ab initio calculation of real solids via neural network ansatz. *Nature Communications* **13**(1), 7895 (2022)
- [30] Pescia, G., Han, J., Lovato, A., Lu, J., Carleo, G.: Neural-network quantum states for periodic systems in continuous space. *Phys. Rev. Res.* **4**, 023138 (2022) <https://doi.org/10.1103/PhysRevResearch.4.023138>
- [31] Wilson, M., Moroni, S., Holzmann, M., Gao, N., Wudarski, F., Vegge, T., Bhowmik, A.: Neural network ansatz for periodic wave functions and the homogeneous electron gas. *Phys. Rev. B* **107**, 235139 (2023) <https://doi.org/10.1103/PhysRevB.107.235139>
- [32] Cassella, G., Sutterud, H., Azadi, S., Drummond, N.D., Pfau, D., Spencer, J.S., Foulkes, W.M.C.: Discovering quantum phase transitions with fermionic neural networks. *Phys. Rev. Lett.* **130**, 036401 (2023) <https://doi.org/10.1103/PhysRevLett.130.036401>
- [33] Pescia, G., Nys, J., Kim, J., Lovato, A., Carleo, G.: Message-passing neural quantum states for the homogeneous electron gas. *arXiv preprint arXiv:2305.07240* (2023)
- [34] Qian, Y., Fu, W., Ren, W., Chen, J.: Interatomic force from neural network based variational quantum monte carlo. *The Journal of Chemical Physics* **157**(16), 164104 (2022)
- [35] Li, X., Qian, Y., Chen, J.: Electric Polarization from Many-Body Neural Network Ansatz (2023)

- [36] Li, X., Fan, C., Ren, W., Chen, J.: Fermionic neural network with effective core potential. *Physical Review Research* **4**, 013021 (2022) <https://doi.org/10.1103/PhysRevResearch.4.013021>
- [37] Wilson, M., Gao, N., Wudarski, F., Riefel, E., Tubman, N.M.: Simulations of state-of-the-art fermionic neural network wave functions with diffusion monte carlo. *arXiv preprint arXiv:2103.12570* (2021)
- [38] Scherbela, M., Reisenhofer, R., Gerard, L., Marquetand, P., Grohs, P.: Solving the electronic schrödinger equation for multiple nuclear geometries with weight-sharing deep neural networks. *Nature Computational Science* (2022) <https://doi.org/10.1038/s43588-022-00228-x>
- [39] Gao, N., Günnemann, S.: Ab-initio potential energy surfaces by pairing GNNs with neural wave functions. In: *International Conference on Learning Representations* (2022). <https://openreview.net/forum?id=apv504XsysP>
- [40] Gao, N., Günnemann, S.: Sampling-free inference for ab-initio potential energy surface networks. In: *The Eleventh International Conference on Learning Representations* (2023). <https://openreview.net/forum?id=Tuk3Pqaizx>
- [41] Gao, N., Günnemann, S.: Generalizing neural wave functions. *arXiv preprint arXiv:2302.04168* (2023)
- [42] Scherbela, M., Gerard, L., Grohs, P.: Towards a foundation model for neural network wave-functions. *arXiv preprint arXiv:2303.09949* (2023)
- [43] Hermann, J., Schätzle, Z., Szabó, P.B., Mežera, M., DeepQMC Contributors: DeepQMC. <https://doi.org/10.5281/zenodo.7503172> . <https://github.com/deepqmc/deepqmc>
- [44] Vicentini, F., Hofmann, D., Szabó, A., Wu, D., Roth, C., Giuliani, C., Pescia, G., Nys, J., Vargas-Calderón, V., Astrakhansev, N., Carleo, G.: NetKet 3: Machine Learning Toolbox for Many-Body Quantum Systems. *SciPost Phys. Codebases*, 7 (2022) <https://doi.org/10.21468/SciPostPhysCodeb.7>
- [45] Wang, C., Li, S., He, D., Wang, L.: Is L^2 physics informed loss always suitable for training physics informed neural network? In: *Advances in Neural Information Processing Systems* (2022). <https://openreview.net/forum?id=cy1TKLRAEML>
- [46] Raissi, M., Perdikaris, P., Karniadakis, G.E.: Physics-informed neural networks: A deep learning framework for solving forward and inverse problems involving nonlinear partial differential equations. *Journal of Computational Physics* **378**, 686–707 (2019)
- [47] He, D., Li, S., Shi, W., Gao, X., Zhang, J., Bian, J., Wang, L., Liu, T.-Y.: Learning physics-informed neural networks without stacked back-propagation. In: *International Conference on Artificial Intelligence and Statistics*, pp. 3034–3047 (2023). PMLR
- [48] Mulliken, R.S.: Electronic population analysis on LCAO–MO molecular wave functions. i. *The Journal of chemical physics* **23**(10), 1833–1840 (1955)
- [49] Paszke, A., Gross, S., Chintala, S., Chanan, G., Yang, E., DeVito, Z., Lin, Z., Desmaison, A., Antiga, L., Lerer, A.: Automatic differentiation in pytorch (2017)
- [50] Abadi, M., Barham, P., Chen, J., Chen, Z., Davis, A., Dean, J., Devin, M., Ghemawat, S., Irving, G., Isard, M., *et al.*: Tensorflow: a system for large-scale machine learning. In: *Osd*, vol. 16, pp. 265–283 (2016). Savannah, GA, USA
- [51] Botev, A.: The gauss-newton matrix for deep learning models and its applications. PhD thesis, UCL (University College London) (2020)
- [52] Martens, J., Sutskever, I., Swersky, K.: Estimating the hessian by back-propagating curvature. *arXiv preprint arXiv:1206.6464* (2012)
- [53] Brown, M.D., Trail, J.R., López Ríos, P.,

Needs, R.J.: Energies of the first row atoms from quantum Monte Carlo. The Journal of Chemical Physics **126**(22), 224110 (2007)
<https://doi.org/10.1063/1.2743972>

Supplementary information of “Forward Laplacian: A New Computational Framework for Neural Network-based Variational Monte Carlo”

Ruichen Li et al

Supplementary Note 1. Hyperparameters

Supplementary Table 1 gives the network architecture hyperparameters for each NN-VMC ansatz. The default hyperparameters for all calculations reported in the main text are mainly listed in Supplementary Table 2. The variations in hyperparameters are shown in Supplementary Table 3.

Supplementary Table 1 | Architecture hyperparameter for different NN-VMC models

Parameter	FermiNet	Psiformer	LapNet
Determinants	16	16	16
Network layers	4	4	4
Attention heads	–	4	4
Attention dimension	–	64	64
MLP hidden dimension	(256, 32)	256	256

Supplementary Table 2 | Default hyperparameters

	Parameter	Value
Training	Optimizer	KFAC
	Iterations	2e5
	Learning rate at iteration t	$lr_0/(1 + \frac{t}{t_0})$
	Initial learning rate lr_0	0.05
	Learning rate decay t_0	1e4
Pretraining	Local energy clipping	5.0
	Optimizer	LAMB
MCMC	Learning rate	1e-3
	Decorrelation steps	30
KFAC	Proposal standard deviation	0.02
	Norm constraint	1e-3
	Damping	1e-3
	Momentum	0
	Covariance moving average decay	0.95

Supplementary Table 3 | Variations in hyperparameters between calculations

	Number of electrons n	Pretraining iterations	MCMC blocks	Pretraining basis set	Batch size
Molecules	$n < 42$	5e3	1	cc-pVDZ	4096
	$42 \leq n < 84$	2e4	2		
	$n \geq 84$	5e4	4		
Ionization potential	any	5e3	1	cc-pVTZ	8192
Barrier height	any	2e4	1	aug-cc-pVDZ	4096
Interaction energy	$n < 42$	5e3	1	aug-cc-pVDZ	4096
	$42 \leq n < 84$	2e4	2		
	$n \geq 84$	5e4	4		

Supplementary Note 2. Systems

The configurations of molecules studied in Fig. 3a can be found in [1, 2]. The reactions we studied in Fig. 4b are listed in Supplementary Table 4 and the corresponding configurations can be found in [3]. The non-covalent systems we studied in Fig. 4c are listed in Supplementary Table 5 and the corresponding configurations can be found in [4].

Supplementary Table 4 | Reactions in Fig. 4b

	Reaction	Type
1	$\text{H} + \text{N}_2\text{O} \longrightarrow \text{OH} + \text{N}_2$	Heavy-atom transfer reaction
2	1 reverse	
3	$\text{H} + \text{FH} \longrightarrow \text{HF} + \text{H}$	
4	$\text{F}^- \dots \text{CH}_3\text{F} \longrightarrow \text{FCH}_3 \dots \text{F}^-$	Nucleophilic substitution reaction
5	$\text{Cl}^- \dots \text{CH}_3\text{Cl} \longrightarrow \text{ClCH}_3 \dots \text{Cl}^-$	
6	$\text{H} + \text{C}_2\text{H}_4 \longrightarrow \text{C}_2\text{H}_5$	Unimolecular and association reaction
7	$\text{C}_2\text{H}_5 \longrightarrow \text{H} + \text{C}_2\text{H}_4$	
8	$\text{HCN} \longrightarrow \text{HNC}$	
9	8 reverse	
10	$s\text{-trans } cis\text{-C}_5\text{H}_8 \longrightarrow s\text{-trans } cis\text{-C}_5\text{H}_8$	
11	$\text{NH}_2 + \text{CH}_3 \longrightarrow \text{NH} + \text{CH}_4$	Hydrogen transfer reaction
12	11 reverse	
13	$\text{NH}_2 + \text{C}_2\text{H}_5 \longrightarrow \text{NH} + \text{C}_2\text{H}_6$	
14	13 reverse	

Supplementary Table 5 | Systems in Fig. 4c

system	Type
1 Water dimer	Hydrogen-bonding interaction system
2 Formic acid dimer	
3 Formamide dimer	
4 Uracil dimer h-bonded	
5 Methane dimer	Dispersion interaction system
6 Ethene dimer	
7 Uracil dimer stack	
8 Ethene ethyne complex	Mixed electrostatic dispersion interaction system
9 Benzene water complex	
10 Benzene dimer T-shaped	
11 Phenol dimer	

Supplementary Note 3. Energy results

This note provides the energy results plotted in Fig. 3a and Fig. 4.

Supplementary Table 6 | Molecules energy in Fig. 3a. The results of FermiNet and Psiformer are from [2].

System	HF, aug-cc-pVDZ	Psiformer[2]	FermiNet[2]	LapNet
LiH	-7.98416	-8.070528(5)	-8.07050(1)	-8.070523(4)
Li ₂	-14.86984	-14.99486(1)	-14.99480(2)	-14.99485(1)
NH ₃	-56.20514	-56.56367(2)	-56.56347(4)	-56.56359(2)
CH ₄	-40.19963	-40.51454(2)	-40.51430(3)	-40.51445(2)
CO	-112.75173	-113.32416(4)	-113.32354(7)	-113.32417(4)
N ₂	-108.96104	-109.54137(4)	-109.54046(6)	-109.54128(4)
C ₂ H ₄	-78.04351	-78.58762(3)	-78.58604(5)	-78.58721(4)
methylamine	-95.23044	-95.86050(4)	-95.85917(6)	-95.86025(3)
O ₃	-224.27901	-225.43061(9)	-225.4226(2)	-225.4293(1)
ethanol	-154.10515	-155.04656(7)	-155.0419(1)	-155.04563(6)
bicyclobutane	-154.88814	-155.94619(8)	-155.9388(1)	-155.94528(4)
benzene	-230.7280	-232.2400(1)	-232.2205(2)	-232.2389(1)
toluene	-269.7684	-271.5538(1)	-271.5274(2)	-271.5524(1)
naphthalene	-383.3934	-385.8685(2)	-385.8147(4)	-385.8655(2)
CCl ₄	-1875.8507	-1878.804(1)	-1878.684(1)	-1878.839(1)
benzene dimer	-461.4555	-464.4667(2)	-464.3770(5)	-464.4681(1)

Supplementary Table 7 | Ionization potential of 5 transition metals in Fig. 4a

System	Atom	Ion	Ionization potential	Experiments[5]
V	-943.8773(1)	-943.6412(1)	0.2361(2)	0.23733
Fe	-1263.6586(2)	-1263.3743(2)	0.2843(3)	0.2871
Co	-1382.7192(1)	-1382.4487(1)	0.2705(2)	0.27137
Ni	-1508.2694(2)	-1508.0117(2)	0.2577(2)	0.25864
Zn	-1779.4364(2)	-1779.1017(3)	0.3347(4)	0.3383

Supplementary Table 8 | Barrier heights of 14 reactions in Fig. 4b

	Reactants	Transition state	Barrier height	W2-F12[3]
1	-185.17156(5)	-185.14391(5)	0.02765(7)	0.02821
2	-185.27710(4)	-185.14391(5)	0.13319(6)	0.13163
3	-100.95854(3)	-100.89248(2)	0.06606(4)	0.06709
4	-239.62929(5)	-239.60805(7)	0.02124(9)	0.02135
5	-960.3632(5)	-960.3388(5)	0.0244(7)	0.02151
6	-79.08694(2)	-79.08432(2)	0.00262(3)	0.00319
7	-79.15115(2)	-79.08432(2)	0.06683(3)	0.06693
8	-93.43241(1)	-93.35566(2)	0.07675(3)	0.07665
9	-93.40824(2)	-93.35566(2)	0.05258(3)	0.05259
10	-195.30143(7)	-195.23616(7)	0.0653(1)	0.06327
11	-95.71460(2)	-95.70018(3)	0.01442(3)	0.01418
12	-95.73547(2)	-95.70018(3)	0.03529(3)	0.03506
13	-135.02977(3)	-135.01383(3)	0.01594(5)	0.01562
14	-135.04518(4)	-135.01383(3)	0.03135(5)	0.03092

Supplementary Table 9 | Interaction energies of 11 systems in Fig. 4c

	System	Equilibrium	Dissociated	Interaction	CCSD(T)/CBS[6]
1	Water dimer	-152.88309(6)	-152.87584(3)	0.00725(8)	0.00795
2	Formic acid dimer	-379.5638(1)	-379.5374(1)	0.0264(2)	0.02988
3	Formamide dimer	-339.8195(1)	-339.79692(8)	0.0226(1)	0.02560
4	Uracil dimer h-bonded	-829.6199(3)	-829.5829(3)	0.0370(4)	0.03289
5	Methane dimer	-81.02888(8)	-81.02861(2)	0.0003(1)	0.00084
6	Ethene dimer	-157.17415(7)	-157.17258(5)	0.0016(1)	0.00235
7	Uracil dimer stack	-829.5946(3)	-829.5829(3)	0.0117(4)	0.01563
8	Ethene-ethyne complex	-155.92198(6)	-155.92068(5)	0.00130(8)	0.00238
9	Benzene-water complex	-308.6756(1)	-308.6727(1)	0.0029(2)	0.00522
10	Benzene dimer T-shape	-464.4681(1)	-464.4655(1)	0.0026(1)	0.00433
11	Phenol dimer	-614.9097(2)	-614.9017(2)	0.0080(3)	0.01131

Supplementary References

- [1] D. Pfau, J.S. Spencer, A.G. de G. Matthews, and W.M.C. Foulkes. Ab-initio solution of the many-electron schrödinger equation with deep neural networks. *Physical Review Research*, 2:033429, 2020.
- [2] Ingrid von Glehn, James S Spencer, and David Pfau. A self-attention ansatz for ab-initio quantum chemistry. In *The Eleventh International Conference on Learning Representations*, 2023.

- [3] Lars Goerigk, Andreas Hansen, Christoph Bauer, Stephan Ehrlich, Asim Najibi, and Stefan Grimme. A look at the density functional theory zoo with the advanced gmtkn55 database for general main group thermochemistry, kinetics and noncovalent interactions. *Physical Chemistry Chemical Physics*, 19:32184–32215, 2017.
- [4] Petr Jurečka, Jiří Šponer, Jiří Černý, and Pavel Hobza. Benchmark database of accurate (MP2 and CCSD (T) complete basis set limit) interaction energies of small model complexes, DNA base pairs, and amino acid pairs. *Physical Chemistry Chemical Physics*, 8(17):1985–1993, 2006.
- [5] Nikolai B. Balabanov and Kirk A. Peterson. Basis set limit electronic excitation energies, ionization potentials, and electron affinities for the 3d transition metal atoms: Coupled cluster and multireference methods. *The Journal of Chemical Physics*, 125(7):074110, 08 2006.
- [6] Michael S. Marshall, Lori A. Burns, and C. David Sherrill. Basis set convergence of the coupled-cluster correction, $\delta_{\text{MP2}}^{\text{CCSD(T)}}$: Best practices for benchmarking non-covalent interactions and the attendant revision of the S22, NBC10, HBC6, and HSG databases. *The Journal of Chemical Physics*, 135(19), 11 2011.